

# Adversarial Shape Learning for Building Extraction in VHR Remote Sensing Images

Lei Ding, Hao Tang, Yahui Liu, Yilei Shi and Lorenzo Bruzzone, *Fellow, IEEE*

**Abstract**—Building extraction in VHR RSIs remains to be a challenging task due to occlusion and boundary ambiguity problems. Although conventional convolutional neural networks (CNNs) based methods are capable of exploiting local texture and context information, they fail to capture the shape patterns of buildings, which is a necessary constraint in the human recognition. In this context, we propose an adversarial shape learning network (ASLNet) to model the building shape patterns, thus improving the accuracy of building segmentation. In the proposed ASLNet, we introduce the adversarial learning strategy to explicitly model the shape constraints, as well as a CNN shape regularizer to strengthen the embedding of shape features. To assess the geometric accuracy of building segmentation results, we further introduced several object-based assessment metrics. Experiments on two open benchmark datasets show that the proposed ASLNet improves both the pixel-based accuracy and the object-based measurements by a large margin. The code is available at: <https://github.com/ggsDing/ASLNet>.

**Index Terms**—Building Extraction, Generative Adversarial Networks (GANs), Image Segmentation, Convolutional Neural Network, Deep Learning, Remote Sensing

## I. INTRODUCTION

The automatic extraction of buildings in very high resolution (VHR) remote sensing images (RSIs) is meaningful for a variety of applications, such as land-cover mapping, urban resources management, the detection of illegal constructions, etc. Conventional building extraction algorithms that extract handcrafted features often fail to perceive high-level context information and are highly dependent on parameters. Recently with the emergence of convolutional neural networks (CNNs) and their applications in semantic segmentation tasks (e.g., vehicle navigation [1], scene sparsing [2], medical image segmentation [3]), great research interests have been drawn to adapt these CNN models for the building extraction in VHR RSIs. The CNN-based building extraction methods employ stacked convolution operations to extract the intrinsic information of image contents, thus a more effective in exploiting the context information and is less sensitive to domain changes. A variety of CNN designs for semantic segmentation tasks have been introduced to segment buildings and are proved to be effective [4], [5].

However, some of the challenges in building extraction remain unsolved even with the use of the recent CNN-based methods. First, occlusions (caused by trees and shadows) and

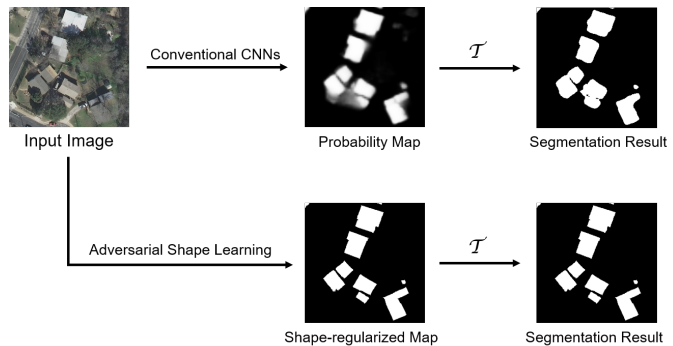


Fig. 1: Illustration of the benefits of the proposed shape learning. Conventional CNN models lead to boundary ambiguity problems, whereas the proposed method produces shape-regularized results.

intra-class divers widely exist in VHR RSIs, which often cause fragmentation and incomplete-segmentation. Second, boundary ambiguity problems. Due to the effects of shadows and building profiles, accurate localization of the building boundaries is difficult (especially in the low-contrast areas). Conventional CNN-based methods produce only probability values in these ambiguous areas, which often cause rounded or uneven building boundaries after thresholding. Last but not least, over-segmentation and under-segmentation of the building objects due to these fragmentation and boundary-adhesion problems. Due to these limitations, post-processing algorithms are often required to optimize the building extraction results [6], [7].

Moreover, previous works on CNN-based building extraction pay more attention to the extraction of texture and context information in RSIs, whereas the explicit modeling of building shapes has rarely been studied. In most cases, buildings in VHR RSIs are compact and rectangular objects with sharp edges and corners. Their rectangularity is very discriminative compared to other ground objects. Learning this shape prior is beneficial for not only inpainting the occluded building parts but also reducing the boundary ambiguities and regularizing the segmentation results. An example is shown in Fig. 1 to illustrate the limitations of conventional CNNs and the benefits of the shape modelling.

In this work, we aim to improve the extraction of buildings by introducing the adversarial learning of their shape information. The main contributions of this work are as follows:

- 1) Proposing an adversarial shape learning network (ASLNet) to learn shape-regularized building extraction

L. Ding, H. Tang, Y. Liu and L. Bruzzone are with the Department of Information Engineering and Computer Science, University of Trento, 38123 Trento, Italy (E-mail: lei.ding@unitn.it, hao.tang@unitn.it, yahui.liu@unitn.it, lorenzo.bruzzone@unitn.it).

This work is supported by the scholarship from China Scholarship Council under the grant NO.201703170123

results. Several strategies are introduced in the designed shape discriminator to exclude the redundant information and focus on modelling the shape information;

- 2) Introducing a CNN shape regularizer to explicitly model the shape features. The dilated convolution and deformable convolutions are introduced in the designed shape regularizer to enlarge the RFs and to learn the local shape patterns in feature maps;
- 3) Designing three object-based assessment measurements to quantitatively evaluate the geometric properties of the building extraction results. These metrics take into account both the under-segmentation and over-segmentation problems and the shape errors of the predicted building items.

The remainder of this paper is organized as follows. Section II introduces the related works on building extraction and adversarial learning. Section III illustrates the proposed ASLNet. Section IV describes the implementation details and the experimental settings. Section V presents the results and analyzes the effect of the proposed method. Section VI draws the conclusions of this study.

## II. RELATED WORK

### A. CNN-based Building Extraction

Literature work on using CNN for building extraction can be roughly divided into three types based on the studied perspectives: supervisions, architecture designs and the development of post-processing algorithms. To begin with, while binary ground truth maps are widely used to compute the segmentation losses, several works have explored the use of other forms of supervisions. In [8], the supervision of signed distance map (SDM) is introduced to highlight the difference between building boundaries and inner structures. In [9] signed distance labels are also introduced but in the form of classification supervision. This SDM has also been used in [10] as an auxiliary supervision.

Most CNN models for building extraction are variants of the well-known architectures for image classification and semantic segmentation. In [4] the ResUNet has been introduced for building extraction from VHR RSIs, which combines ResNet [11] with the UNet [3] structure. The MFCNN in [6] is also a symmetric CNN with ResNet as the feature extractor, whereas it contains more sophisticated designs (such as dilated convolution units and the pyramid feature fusion). In [12] a Siamese UNet with two branches is designed to extract buildings from different spatial scales. In [13] a hybrid network with multiple sub-nets is introduced to exploit information from the multi-source input data. In [5] the MAPNet is proposed, which is a HRNet-like architecture with multiple feature encoding branches and channel attention designs. In [14] the global multi-scale encoder-decoder network (GMEDN) is proposed, which consists of a UNet-like network and a non-local modelling unit.

Since conventional CNN models only produce coarse segmentation results, post-processing operations are often required to obtain finer results. In [4] guided filters are used to optimize the segmented building boundaries and to remove

noise. In [7] and [15] regularization algorithms are developed to refine the segmentation maps. These algorithms perform object-based analysis on the edges and junction points to generate building-like polygons. In [6], a regularization algorithm is designed based on morphological operations on the rotated segmentation items.

### B. Adversarial Learning

1) *Generative Adversarial Networks (GANs) [16]*: GANs typically consist of two important components: a generator and a discriminator. The aim of the generator is to generate realistic results from the input data, while the discriminator is used to distinguish between the real data and the generated one. Since the discriminator is also a CNN, it is capable of learning the intrinsic differences between the real and fake data, which can hardly be modeled by human-defined algorithms. Therefore, the GANs have been widely used for a variety of complex tasks in the computer vision field, such as image generation [17], [18], [19], [20], semantic segmentation [21], [22], object detection [23], [24], depth estimation [25], and image/action recognition [26], [27].

2) *Adversarial Learning for Building Extraction*: Several literature works have introduced the adversarial learning strategy for building extraction. The segmentation model can be seen as a generative network, thus the building segmentation results can be learned in an adversarial manner by employing a CNN discriminator. The work in [28] is an early attempt on using the adversarial learning for building extraction. It forwards the masked input RSIs to the discriminator and uses an auto-encoder to reconstruct it. In [29] the GAN has been used to generate synthetic depth maps, thus improving the accuracy of building segmentation. In [30] the generative adversarial learning is introduced to improve the accuracy of building segmentation, which employs a discriminator to discriminate whether the segmentation map is the ground truth (GT) map or the segmentation results. In [31] a multi-scale L1 loss is calculated from the discriminator to train the segmentation network. In [32] a cwGAN-GP is proposed for building segmentation, which combines the CGAN and WGAN and introduces a gradient penalty term.

To conclude, the literature works on using adversarial learning for building extraction generally combine the segmentation maps and the RSIs as input data to the discriminator, whereas the shape of segmented items has not been exploited.

### C. CNN-based Shape modelling

There are limited number of works on CNN-based modelling of 2D shapes. To begin with, the work in [33] shows that CNNs can recognize shapes in binary images with high accuracy. In [34] the modelling of shape information is studied for the segmentation of kidneys from ultrasound scan images. In this work, a CNN auto-encoder is introduced to regularize the CNN output, which is pre-trained to recover the intact shape from randomly corrupted shapes. The shape regularization network is trained by three loss terms that measure the distance between the input segmentation map, regularized segmentation map, and the ideal segmentation map. In [35] a

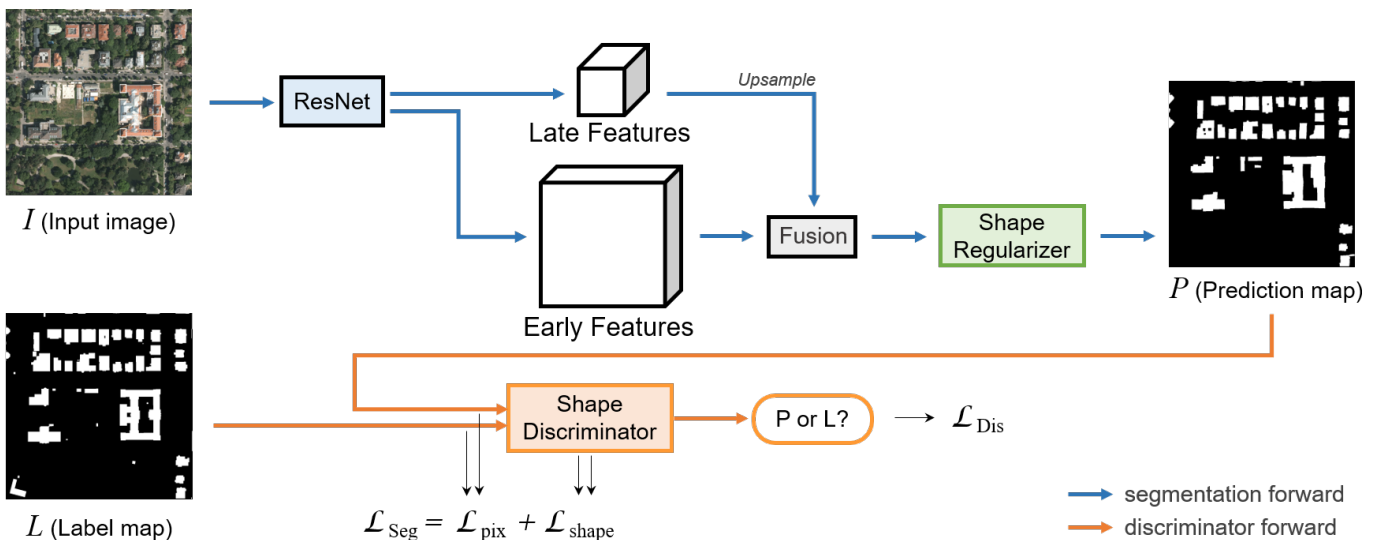


Fig. 2: The proposed Adversarial Shape Learning Network (ASLNet) for building extraction. We designed an explicit shape regularizer to model the shape features, and a shape discriminator to guide the segmentation network.

gated shape CNN is proposed for the semantic segmentation. It contains an explicit shape stream that deals with the object boundary information.

Several works use binary mask features to preserve and model the shape information. In [36], the shape priors are modeled to improve the instance segmentation. The label masks are cluttered to generate class-wise shape priors. These priors are then weighted by a learnt vector of parameters to estimate the coarse instance region. In [37], a shape-variant convolution is proposed for the semantic segmentation. It uses a novel paired convolution to learn context-dependent masks to limit the receptive fields (RFs) on interested image regions. In [38], the modeling of object contour polygons is studied for the instance segmentation. The polygons are first generated with a segmentation CNN and then transformed in a transformer network to fit to the object contours.

To the best of our knowledge, there is no existing work that uses the adversarial learning strategy to explicitly model the shape information.

### III. ADVERSARIAL SHAPE LEARNING NETWORK

Typical CNN models [4], [6] for building segmentation exploit only the local texture and context information, thus the fragmentation and boundary ambiguity problems remain unsolved. Since buildings in VHR RSIs usually have clear shape patterns, it is meaningful to utilize the shape constraints to alleviate these problems. To this end, we propose the adversarial shape learning network (ASLNet) to explicitly model these shape constraints. In this section, we describe in detail the architecture, loss functions, and the CNN modules of our ASLNet.

#### A. Network Architecture

Fig. 2 illustrates the architecture of the proposed ASLNet for building extraction, which consists of a segmentation network and a discriminator network. The segmentation network

is designed following the encoder-decoder structure in [39] and [40]. The choice of the backbone network for feature extraction is not the focus of this work, thus we simply adopt the ResNet [41] in the encoder. It has been widely used as feature extraction network in building segmentation [42], road segmentation [43], and other semantic segmentation related tasks [44]. The selected ResNet version is ResNet34, which can be replaced by other versions based on the complexity of the dataset.

Apart from the output features from the late layers of the ResNet (with 1/8 of the original GSD), the early features (with 1/2 of the original GSD) are also employed in the decoder to learn finer spatial details. This ResNet with encoder-decoder structure is a modified version of FCN [2], denoted as ED-FCN. It is set as the baseline network for comparisons. Furthermore, a shape regularizer is designed at the end of the segmentation network of the proposed ASLNet to produce shape-refined outputs.

#### B. Shape Regularizer

Although using a simple ResNet as the segmentation network is feasible for the adversarial shape learning, it is beneficial to model the shape features at finer spatial scales. Therefore, we design an explicit shape regularizer in the decoder of the segmentation network to enable a better adaptation to the shape constraints (see Fig. 3). The shape regularizer is placed at the spatial scale of 1/4 of the GSD, whose input features are fused multiscale features of the ResNet. At this spatial scale, a conventional  $3 \times 3$  convolutional kernel has the RF of around  $12 \times 12$  pixels, which is too small for modelling the local shape patterns. Therefore, we introduce the dilated convolution (DC) and deformable convolution (DFC) [45] layers to enlarge the RFs and to learn shape-sensitive transformations.

Both the DC and DFC are based on the idea of enlarging the coverage of convolutional kernels. Denote a convolutional

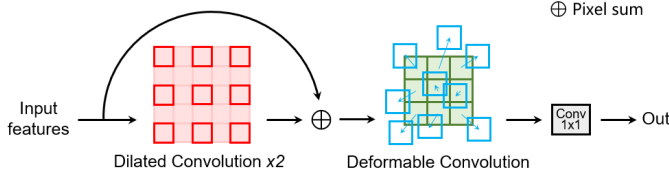


Fig. 3: The designed shape regularizer. Dilated convolutions and deformable convolutions are employed to enlarge the RFs and learn the shape features.

operation for pixel  $x(r, c)$  as:

$$U(r, c) = \sum_{i,j} x_{r+i,c+j} \cdot k_{i,j}, \quad (1)$$

where  $k_{i,j}$  denotes the kernel weight. In a standard  $3 \times 3$  convolution,  $i, j \in \{-1, 0, 1\}$ . In a  $3 \times 3$  DC, however,  $i, j \in \{-r, 0, r\}$  where  $r$  is the dilation rate. In the designed shape regularizer we connected two  $3 \times 3$  DCs as a residual block [11], which enlarges the RF to over  $36 \times 36$  pixels. A DFC is further employed to exploit the shape information, denoted as:

$$U_{df}(r, c) = \sum_{i,j} x_{r+i+u(r,c),c+j+v(r,c)} \cdot k_{i,j}, \quad (2)$$

where  $u(r, c)$  and  $v(r, c)$  are position parameters learned by the additional convolutions:

$$u(r, c) = \sum_{i,j} x_{r+i,c+j} \cdot k'_{i,j}, v(r, c) = \sum_{i,j} x_{r+i,c+j} \cdot k''_{i,j}. \quad (3)$$

This enables the shape regularizer to perceive and adapt to the local shape patterns. Finally, a  $1 \times 1$  convolution is followed to merge the features into a segmentation map.

### C. Shape Discriminator

Although several literature works have introduced the adversarial learning for building extraction, most of them combine CNN outputs and input RSIs to train the discriminators [32], [29], [30], [31]. Under this circumstance, the discriminators are unlikely to learn the shape information, since they are effected by the redundant information in input RSIs. In the proposed ASLNet, the discriminator focuses on only the shape features, thus we exclude the use of input RSIs.

However, training a shape discriminator with only binary inputs faces technical problems. Denote  $P$  as an output map of the segmentation network and  $L$  as its corresponding ground truth label. In typical binary segmentation methods, the building extraction result  $R = \mathcal{T}[\sigma(P)]$ , where  $\sigma$  is the Sigmoid function and  $\mathcal{T}$  is a thresholding or argmax function. In most cases,  $\mathcal{T}$  is non-differential, thus calculating  $\mathcal{L}_{Seg}$  with  $R$  and  $L$  will lead to zero-gradient problems. In literature works [28] this problem remains unsolved. Although calculating  $\mathcal{L}_{Seg}$  directly with  $\sigma(P)$  and  $L$  is a feasible alternative, the value range of  $\sigma(P) \in [0, 1]$  and  $L \in \{0, 1\}$  is significantly different. This difference can be easily captured by the discriminator and causes failure to the shape modelling.

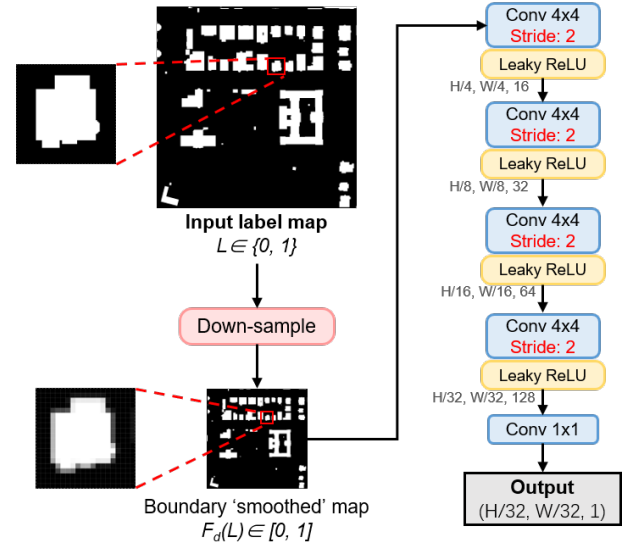


Fig. 4: The designed shape discriminator. The input maps are down-scaled to exclude the impact of ‘hard’ building boundaries in reference maps.

In the designed shape discriminator we solve this problem by adding a down-sampling operation  $F_d$ . Fig. 4 illustrates the designed shape discriminator. After applying  $F_d$ , the building boundaries on  $F_d(L)$  are ‘softened’ ( $F_d(L) \in [0, 1]$ ) and the value difference between  $F_d(\sigma(P))$  and  $F_d(L)$  is excluded. Specifically, four layers of strided convolution and activation functions are then employed to reduce the spatial size of feature maps and learn the local discriminative shape information. The output results are related to  $1/32$  of the original GSD.

The discriminator is trained with the Binary Cross Entropy (BCE) loss function. It is calculated as:

$$\begin{aligned} \mathcal{L}_{Dis} &= \mathbb{E}_{L \sim p_{data}(L)} [\log \mathcal{D}(L)] \\ &+ \mathbb{E}_{P \sim P_{data}(P)} [\log(1 - \mathcal{D}(\sigma(P)))] \\ &= -y \log(p) - (1 - y) \log(1 - p), \end{aligned} \quad (4)$$

where  $y$  denotes the encoded signal that whether the input map to the discriminator is  $L$  or  $\sigma(P)$  (‘1’ and ‘0’, respectively),  $p$  is the output of the discriminator. In typical GANs the BCE loss is also used to supervise the generator network. In experimental practice, however, we found that this leads to training insatiability problems. As an alternative, we employ the Mean Squared Error (MSE) loss function to calculate the  $\mathcal{L}_{Shape}$  as:

$$\mathcal{L}_{Shape} = \{\mathcal{D}(L) - \mathcal{D}[\sigma(P)]\}^2, \quad (5)$$

where  $\mathcal{D}$  is the shape discriminator.

### D. Optimization Objective of ASLNet

Denote  $\mathcal{L}_{Seg}$  as the loss function for the CNN-based segmentation of buildings. In conventional CNNs,  $\mathcal{L}_{Seg}$  is only related to the pixel-wise accuracy, which does not consider the image context. At the end of shape learning via CNNs, it is essential to define a shape-based loss function  $\mathcal{L}_{Shape}$ . Previous works on shape analysis are often object-based [46],

[47]. They include non-differential operations to calculate the shape measures, which are difficult to be incorporated into CNNs. Since CNNs themselves can be trained to discriminate different shapes, we introduce the idea of adversarial learning to learn the  $\mathcal{L}_{Shape}$  to guide the segmentation network.

$$\begin{aligned}\mathcal{L}_{Seg} &= \alpha \cdot \mathcal{L}_{Pix} + \beta \cdot \mathcal{L}_{Shape} \\ &= \alpha \cdot [L - \sigma(P)]^2 + \beta \cdot \{\mathcal{D}(L) - \mathcal{D}[\sigma(P)]\}^2,\end{aligned}\quad (6)$$

where  $\mathcal{L}_{Pix} = [L - \sigma(P)]^2$  is the supervised pixel-based reconstruction loss,  $\alpha$  and  $\beta$  are two weighting parameters.

#### IV. EXPERIMENTS

In this section, we describe the experimental dataset, the implementation details, and the evaluation metrics.

##### A. Dataset Descriptions

We conduct building extraction experiments on two VHR RSI datasets, i.e., the Inria dataset [48] and the Massachusetts Building dataset [49]. These are two of the most often used building extraction datasets in literature works [6], [28], [14], [42].

1) *Inria Dataset* [48]: This is an aerial dataset with the GSD of 0.3 m per pixel, covering 810 km<sup>2</sup>. Each image has 5,000 × 5,000 pixels. There are a total of 360 images in this dataset, among which 180 ones are provided with the ground truth labels. These 180 images were collected in five different cities: Austin (U.S.), Chicago (U.S.), Kitsap (U.S.), Tyrol (Austria), and Vienna (Austria). Following the practice in [6][14], we use the first 5 images in each city for testing and the rest 31 images for training.

2) *Massachusetts (MAS) Building Dataset* [49]: This is an aerial dataset collected from the Boston area. It has a GSD of 1.2 m per pixel, covering around 340 km<sup>2</sup>. The imaged regions include urban and suburban scenes where there are buildings with diverse sizes. This dataset consists of a training set with 137 images, a validation set with 4 images, and a testing set with 10 images. Each image has 1,500 × 1,500 pixels.

##### B. Implementation Details

The experiments were conducted on a workstation with 32 GB RAM and a NVIDIA Quadro P6000 GPU (23GB). Since it is impossible to train directly the large RSIs, they are randomly cropped into 512 × 512 patch images during the training process. The performed data preprocessing and augmentation operations include data normalization, random cropping, and image flipping. The training batch size is set to 8 and the number of training epochs are 50. The validation and testing set are evaluated on the original size RSIs to avoid the impact of cropping parameters. The parameters  $\alpha, \beta$  in the Eq. (6) are empirically set to 1.0, 5.0, respectively. This numeric setting is to make the  $\mathcal{L}_{Pix}$  as the primary loss function.

##### C. Evaluation Metrics

1) *Pixel-based Evaluation Metrics*: We adopt several commonly used evaluation metrics in building extraction [6], [10] and other binary segmentation tasks [43] to assess the accuracy of the results. These metrics are based on statistical analysis of the classified pixels, including: overall accuracy (OA), Precision (P), Recall (R), F1 score, and mean Intersection over Union (mIoU). The calculations are:

$$P = \frac{TP}{TP + FP}, \quad R = \frac{TP}{TP + FN}, \quad (7)$$

$$F1 = 2 \times \frac{P \times R}{P + R}, \quad OA = \frac{TP + TN}{TP + FP + TN + FN}, \quad (8)$$

$$IoU = \frac{TP}{TP + FP + FN} \quad (9)$$

where  $TP, FP, TN$ , and  $FN$  represent true positive, false positive, true negative, and false negative, respectively.

2) *Object-based Evaluation Metrics*: Although the pixel-based evaluation metrics present the overall classification accuracy of the results, they fail to consider the thematic and geometrical properties of the segmented units [46]. To overcome this limitation, we designed three object-based evaluation metrics, including the matching rate ( $MR$ ), the curvature error ( $E_{curv}$ ), and the shape error ( $E_{shape}$ ). These metrics are variants of the literature works [50], [47] to adapt to the assessment of building extraction results.

To begin with, in order to compare the geometric proprieties of a segmented object  $S_j$  on the prediction map  $P$  and a reference object  $O_i$  on the GT map  $L$ , it is essential to first discriminate if they are representing the same physical object. For each  $O_i$  ( $i = 1, 2, 3, \dots, n$ ) and  $S_j$  ( $j = 1, 2, 3, \dots, n'$ ), their matching relationship  $M(O_i, S_j)$  is calculated based on the over-segmentation error ( $E_{os}$ ) and under-segmentation error ( $E_{us}$ ) [50]:

$$M(O_i, S_j) = \begin{cases} 0, & E_{os}(O_i, S_j) > T \text{ || } E_{us}(O_i, S_j) > T \\ 1, & E_{os}(O_i, S_j) \leq T \text{ \& } E_{us}(O_i, S_j) \leq T \end{cases} \quad (10)$$

$$E_{os}(O_i, S_j) = 1 - \frac{|S_j \cap O_i|}{|O_i|}, \quad E_{us}(O_i, S_j) = 1 - \frac{|S_j \cap O_i|}{|S_j|}, \quad (11)$$

where  $T$  is empirically set to 0.3. The matching rate ( $MR$ ) of  $P$  is the numeric ratio of the matched objects in  $L$  among all the  $O_i$  in  $L$ :

$$MR = \frac{\sum_{i,j} M(O_i, S_j)}{N_{O_i}} \quad (12)$$

After finding the matched item  $M_i$  in  $P$  for  $O_i$ , two geometric measurements are further calculated to measure the differences between  $M_i$  and  $O_i$ . First,  $E_{curv}$  is introduced to measure the differences in object boundaries. It is calculated as:

$$E_{curv}(O_i, M_i) = \|f_c(M_i) - f_c(O_i)\|, \quad (13)$$

where  $f_c$  denotes the contour curvature function [51]. Since  $O_i$  is human-annotated,  $f_c(O_i)$  is usually small. A large

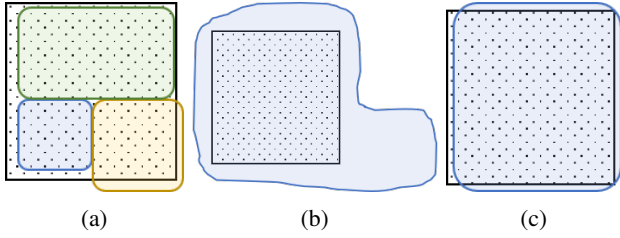


Fig. 5: Illustration of three overlapping relationships between a segmented object  $S_j$  (colored region) and a reference object  $O_i$  (dotted region). (a) over-segmentation, (b) under-segmentation, (c) matching.

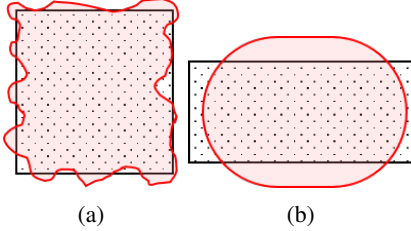


Fig. 6: Examples of the reference object  $O_i$  (dotted region) and its matched segmented object  $M_i$  (colored region) that have: (a) high curvature error ( $E_{curv}$ ), (b) high shape error ( $E_{shape}$ ).

$E_{curv}(O_i, M_i)$  indicates that the boundary of  $f_c(M_i)$  is uneven. The second measurement  $E_{shape}$  is introduced to assess the difference in shape, calculated as:

$$E_{shape}(O_i, M_i) = ||f_s(M_i) - f_s(O_i)||, \quad f_s(M_i) = \frac{4\pi|M_i|}{p_{M_i}^2}, \quad (14)$$

where  $p_{M_i}$  is the perimeter of  $M_i$ . The value of  $f_s(M_i)$  is 1 for a circle and  $\pi/4$  for a square [47], [51].

## V. EXPERIMENTAL RESULTS

This section presents the experimental results obtained on the two VHR building datasets. First, we present the ablation study to quantitatively evaluate the improvements brought by the proposed method. Then the effects of the shape regularizer (SR) and the shape discriminator (SD) are analysed with some results in sample area. Finally, the proposed ASLNet is compared with several state-of-the-art CNN models for building extraction.

### A. Ablation Study

We conduct extensive ablation studies to assess the effectiveness of the proposed ASLNet. To compare the results before and after the use of SR and SD, the original FCN [2] and the baseline method ED-FCN are also included in the comparison. The quantitative results are reported in Table I. The baseline ED-FCN outperforms the FCN in mIoU by 0.21% and 4.87%, respectively in the Inria and the MAS dataset, which is attributed to the concatenation of low-level features in its decoder. Since the MAS dataset has lower spatial resolution, the improvements of the ED-FCN is more

noticeable. After introducing the adversarial shape learning, the ASLNet (without the SR) has the mIoU improvements of 1.56% and 2.63% on the two datasets, respectively. The complete ASLNet with both the SR and the SD have the improvements of 2.73% and 3.06% in mIoU compared to the baseline ED-FCN. Fig.9 show a comparison of the OA values of the segmented probability maps across different thresholds. Since the ASLNet directly segments near-binary regularized results, its OA curves are close to horizontal, and are high above the baseline methods.

The improvements are even more significant in terms of object-based metrics. The baseline FCN encountered severe over-segmentation problems which leads to low  $MR$  values. The ED-FCN improves slightly both the three object-based metrics. The ASLNet (without the SR) has improvements of around 3 in both  $E_{curv}$  and  $E_{shape}$  in the two datasets. The ASLNet (with the SR) has further improved greatly the  $MR$  values.

Fig. 7 shows the results of the ablation study on several sample areas. The segmentation results of the ED-FCN are generally round-edged. After adding the SD, however, the building edges became sharper and the object shapes became more rectangular. After adding further the SD, the object shapes are modelled in a wider image range, thus the edges are more straight and some missing parts are inpainted. More specifically, Fig. 7(a)(e) show two cases of occlusions caused by trees and shadows, respectively. Fig. 7(c) shows a case of under-segmentation. In these cases the ASLNet has successfully recovered the complete buildings. Fig. 7(b)(d)(f) show several examples of the improvements in shapes. The ASLNet managed to improve the segmented shape of both compact small objects (e.g., houses), irregular large object (e.g., factories), and long bar-like objects (e.g., residential buildings). However, a side-effect of the ASLNet is that it fails to segment some round objects (e.g., oil tanks), since the shape constraints drive it to produce rectangular outputs. Some of the failed cases are shown in Fig. 8. Considering that there are usually limited numbers of irregular buildings, this drawback has minor impacts.

As a conclusion of the ablation study, the modeling of shape features in the ASLNet leads to three significant benefits: 1) inpainting of the missing parts of buildings; 2) joint segmentation and regularization of the building contours; 3) alleviation to the under-segmentation and over-segmentation problems. These advantages are verified by both the accuracy metrics and visual observation.

### B. Comparative Experiments

We further compare the proposed ASLNet with several literature works to assess its performance. Three classic models for the semantic segmentation are compared, including the UNet [3], the baseline method FCN [2] and the Deeplabv3+ [39]. Several state-of-the-art methods for the building extraction are also compared, including the ReSUNet [4], the MAPNet [5] and the GMEDN [14]. The quantitative results on the Inria dataset and the MAS dataset are reported in Table.II and Table.III, respectively. Let us first

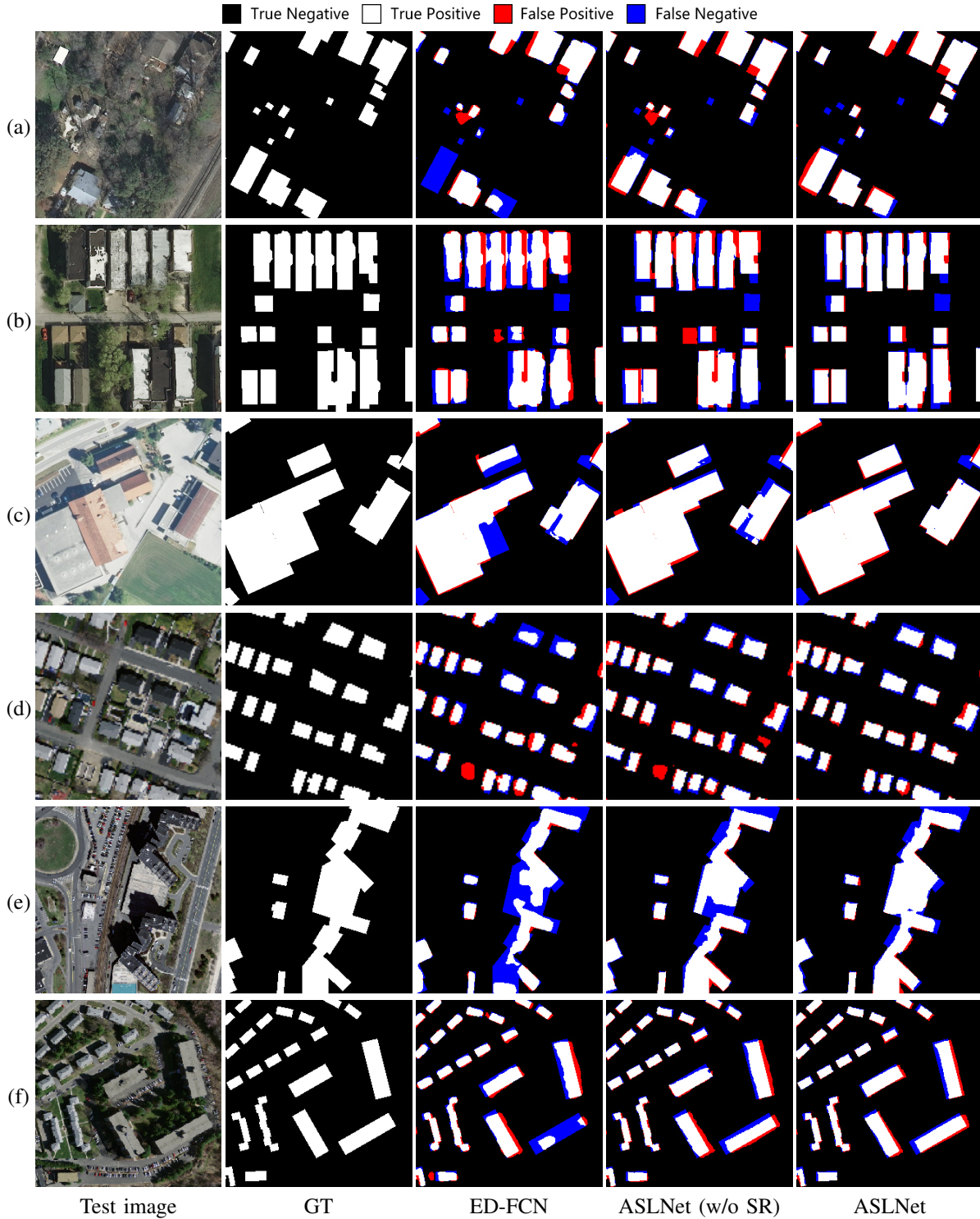


Fig. 7: Examples of the segmentation results (ablation study). (a)-(c) Results selected from the Inria dataset, (d)-(f) Results selected from the Massachusetts dataset.

analyze the pixel-based metrics. The ResUNet, which is a variant of UNet for the building extraction, exceeds the classic semantic segmentation models (UNet, FCN and Deeplabv3+) by a large margin on the MAS dataset. The MAPNet obtains competitive results on the Inria dataset, whereas its performance is inferior to the ResUNet and the Deeplabv3+

on the MAS dataset. The GMEDN, on the contrary, obtains better accuracy on the MAS dataset. The proposed ASLNet outperforms all the compared methods by a large margin, although its baseline method (the ED-FCN) is inferior to most of them. The advantages of the ASLNet are particularly noticeable on the Inria dataset, where the ASLNet has a lead

TABLE I: Results of the ablation study.

Dataset	Method	Components		Pixel-based Metrics					Object-based Metrics		
		SR	SD	OA(%)	P(%)	R(%)	F1(%)	mIoU(%)	MR(%)	$E_{curv}$	$E_{shape}$
Inria	FCN [2]			96.72	89.41	83.78	86.33	76.36	55.37	7.66	6.63
	ED-FCN			96.69	87.87	85.29	86.46	76.57	60.38	7.26	6.29
	ASLNet (w/o SR)		✓	96.94	88.98	86.32	87.50	78.13	60.36	3.86	4.36
	ASLNet	✓	✓	<b>97.15</b>	<b>90.00</b>	<b>86.85</b>	<b>88.27</b>	<b>79.30</b>	<b>64.46</b>	<b>3.53</b>	<b>3.66</b>
MAS	FCN [2]			92.39	78.46	78.73	78.56	64.82	26.87	11.56	7.79
	ED-FCN			93.81	84.83	79.57	82.09	69.69	53.62	8.78	7.45
	ASLNet (w/o SR)		✓	94.38	85.70	81.17	83.91	72.32	62.39	7.36	4.30
	ASLNet	✓	✓	<b>94.46</b>	<b>86.06</b>	<b>82.47</b>	<b>84.20</b>	<b>72.75</b>	<b>66.81</b>	<b>7.07</b>	<b>4.10</b>

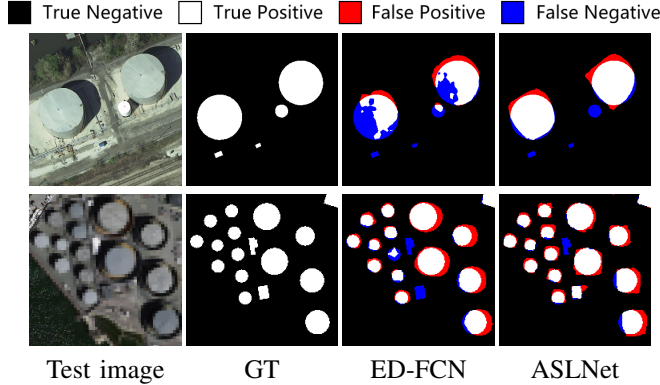


Fig. 8: Examples of the failure cases. The ASLNet segments rectangular items for even the round objects.

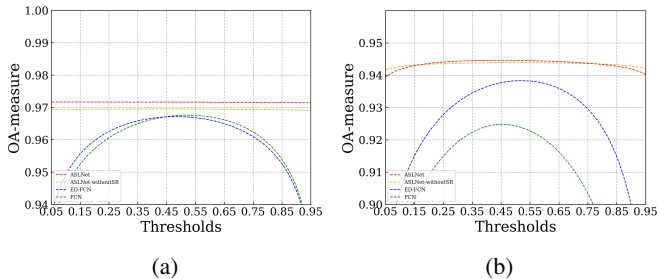


Fig. 9: Accuracy curves across different thresholds. (a) Inria dataset; (b) Massachusetts dataset.

of 1.51% in mIoU.

In terms of object-based metrics, there are remarkable differences in the  $MR$  values. The ResUNet and the Deeplabv3+ obtained the best  $MR$  values among the literature methods on the Inria dataset and the MAS dataset, respectively. However, all the compared literature methods (except for the UNet) obtained similar  $E_{curv}$  and  $E_{shape}$  values. This indicates that they all suffer from irregular shapes and uneven boundaries problems. The proposed ASLNet, however, shows significant advantages in terms of all these three metrics. Due to its learned shape constraints that regularize the segmented items and greatly alleviate the under-segmentation and over-segmentation problems, the ASLNet has advantages of over 5% in  $MR$  and over 2 in  $E_{shape}$  in both datasets.

## VI. CONCLUSIONS

Recent works on CNN-based building extraction exhibit severe limitations on two problems: 1) incomplete segmentation of objects due to occlusion problems; 2) thematic regularization of the building extraction results. To address these problems, we introduce the adversarial training strategy to learn the shape of buildings and propose an ASLNet. Specifically, we designed a shape regularizer to regularize the feature maps, as well as a shape discriminator to guide the segmentation network to learn shape features. To quantitatively evaluate the thematic properties of the building extraction results, we also designed three object-based metrics: the matching rate, the curvature error and the shape error.

Experimental results on two VHR building datasets show that the proposed ASLNet has obtained significant improvements over the conventional CNN models in both pixel-based metrics and object-based metrics. These improvements can be attributed to two factors. First, learning the shape priors is beneficial to inpainting the missing building parts. Second, the shape constraints force the ASLNet to produce shape-regularized results, thus the segmented objects have rectangular shape and smooth boundaries. Additionally, we found that the ASLNet greatly reduces the over-segmentation and under-segmentation problems (proved by the higher  $M$  values). However, one of the problems of the ASLNet is that it segments rectangular items for even the round buildings, which is due to its learned shape constraints.

The adversarial shape learning is potentially beneficial for other segmentation-related tasks with the RSIs, where the ground objects exhibit certain geometric patterns. We will investigate to use the adversarial shape learning to improve the multi-class semantic segmentation and road extraction in VHR RSIs in future studies.

## REFERENCES

- [1] V. Badrinarayanan, A. Kendall, and R. Cipolla, "Segnet: A deep convolutional encoder-decoder architecture for image segmentation," *TPAMI*, vol. 39, no. 12, pp. 2481–2495, 2017.
- [2] J. Long, E. Shelhamer, and T. Darrell, "Fully convolutional networks for semantic segmentation," in *CVPR*, 2015.
- [3] O. Ronneberger, P. Fischer, and T. Brox, "U-net: Convolutional networks for biomedical image segmentation," in *International Conference on Medical image computing and computer-assisted intervention*. Springer, 2015.
- [4] Y. Xu, L. Wu, Z. Xie, and Z. Chen, "Building extraction in very high resolution remote sensing imagery using deep learning and guided filters," *Remote Sensing*, vol. 10, no. 1, p. 144, 2018.



TABLE II: Results of the comparative experiments on the Inria dataset.

Method	Pixel-based Metrics					Object-based Metrics		
	OA(%)	P(%)	R(%)	F1(%)	mIoU(%)	MR(%)	$E_{curv}$	$E_{shape}$
UNet [3]	95.52	81.76	82.76	82.03	70.03	43.87	10.89	7.84
FCN [2]	96.72	89.41	83.78	86.33	76.36	55.37	7.66	6.63
Deeplabv3+ [39]	96.85	89.17	85.09	86.97	77.30	58.63	7.12	6.29
ResUNet [4]	96.50	88.33	83.60	85.68	75.41	55.72	7.47	6.50
MAPNet [5]	96.96	88.58	86.04	87.24	77.79	59.75	6.26	6.16
GMEDN [14]	96.23	87.03	81.37	83.88	72.95	52.65	8.43	5.54
ASLNet (proposed)	<b>97.15</b>	<b>90.00</b>	<b>86.85</b>	<b>88.27</b>	<b>79.30</b>	<b>64.46</b>	<b>3.53</b>	<b>3.66</b>

TABLE III: Results of the comparative experiments on the Massachusetts dataset.

Method	Pixel-based Metrics					Object-based Metrics		
	OA(%)	P(%)	R(%)	F1(%)	mIoU(%)	MR(%)	$E_{curv}$	$E_{shape}$
UNet [3]	92.18	84.71	70.29	76.75	62.34	40.02	10.23	7.10
FCN [2]	92.39	78.46	78.73	78.56	64.82	26.87	11.56	7.79
Deeplabv3+ [39]	93.27	82.28	78.95	80.53	67.52	47.15	9.82	7.67
ResUNet [4]	94.32	86.16	81.25	83.59	71.87	60.22	7.91	7.16
MAPNet [5]	93.47	<b>87.88</b>	72.77	79.50	66.20	53.70	8.05	7.63
GMEDN [14]	93.29	84.09	77.49	80.63	67.61	51.20	9.20	7.26
ASLNet (proposed)	<b>94.46</b>	86.06	<b>82.47</b>	<b>84.20</b>	<b>72.75</b>	<b>66.81</b>	<b>7.07</b>	<b>4.10</b>

- [5] Q. Zhu, C. Liao, H. Hu, X. Mei, and H. Li, "Map-net: Multiple attending path neural network for building footprint extraction from remote sensed imagery," *IEEE Transactions on Geoscience and Remote Sensing*, 2020.
- [6] Y. Xie, J. Zhu, Y. Cao, D. Feng, M. Hu, W. Li, Y. Zhang, and L. Fu, "Refined extraction of building outlines from high-resolution remote sensing imagery based on a multifeature convolutional neural network and morphological filtering," *IEEE Journal of Selected Topics in Applied Earth Observations and Remote Sensing*, vol. 13, pp. 1842–1855, 2020.
- [7] S. Wei, S. Ji, and M. Lu, "Toward automatic building footprint delineation from aerial images using cnn and regularization," *IEEE Transactions on Geoscience and Remote Sensing*, vol. 58, no. 3, pp. 2178–2189, 2019.
- [8] J. Yuan, "Learning building extraction in aerial scenes with convolutional networks," *IEEE transactions on pattern analysis and machine intelligence*, vol. 40, no. 11, pp. 2793–2798, 2017.
- [9] H. L. Yang, J. Yuan, D. Lunga, M. Laverdiere, A. Rose, and B. Bhaduri, "Building extraction at scale using convolutional neural network: Mapping of the united states," *IEEE Journal of Selected Topics in Applied Earth Observations and Remote Sensing*, vol. 11, no. 8, pp. 2600–2614, 2018.
- [10] Y. Shi, Q. Li, and X. X. Zhu, "Building segmentation through a gated graph convolutional neural network with deep structured feature embedding," *ISPRS Journal of Photogrammetry and Remote Sensing*, vol. 159, pp. 184–197, 2020.
- [11] K. He, X. Zhang, S. Ren, and J. Sun, "Deep residual learning for image recognition," in *CVPR*, 2016.
- [12] S. Ji, S. Wei, and M. Lu, "Fully convolutional networks for multisource building extraction from an open aerial and satellite imagery data set," *IEEE Transactions on Geoscience and Remote Sensing*, vol. 57, no. 1, pp. 574–586, 2018.
- [13] K. Bittner, F. Adam, S. Cui, M. Körner, and P. Reinartz, "Building footprint extraction from vhr remote sensing images combined with normalized dsms using fused fully convolutional networks," *IEEE Journal of Selected Topics in Applied Earth Observations and Remote Sensing*, vol. 11, no. 8, pp. 2615–2629, 2018.
- [14] J. Ma, L. Wu, X. Tang, F. Liu, X. Zhang, and L. Jiao, "Building extraction of aerial images by a global and multi-scale encoder-decoder network," *Remote Sensing*, vol. 12, no. 15, p. 2350, 2020.
- [15] K. Zhao, J. Kang, J. Jung, and G. Sohn, "Building extraction from satellite images using mask r-cnn with building boundary regularization," in *Proceedings of the IEEE Conference on Computer Vision and Pattern Recognition Workshops*, 2018, pp. 247–251.
- [16] I. Goodfellow, J. Pouget-Abadie, M. Mirza, B. Xu, D. Warde-Farley, S. Ozair, A. Courville, and Y. Bengio, "Generative adversarial nets," in *NeurIPS*, 2014.
- [17] T. Karras, S. Laine, and T. Aila, "A style-based generator architecture for generative adversarial networks," in *CVPR*, 2019.
- [18] H. Tang, S. Bai, L. Zhang, P. H. Torr, and N. Sebe, "Xinggan for person image generation," in *ECCV*, 2020.
- [19] T. R. Shaham, T. Dekel, and T. Michaeli, "Singan: Learning a generative model from a single natural image," in *ICCV*, 2019.
- [20] H. Tang, W. Wang, D. Xu, Y. Yan, and N. Sebe, "Gesturegan for hand gesture-to-gesture translation in the wild," in *ACM MM*, 2018.
- [21] Y.-H. Tsai, W.-C. Hung, S. Schuler, K. Sohn, M.-H. Yang, and M. Chandraker, "Learning to adapt structured output space for semantic segmentation," in *CVPR*, 2018.
- [22] T.-H. Vu, H. Jain, M. Bucher, M. Cord, and P. Pérez, "Advent: Adversarial entropy minimization for domain adaptation in semantic segmentation," in *CVPR*, 2019.
- [23] J. Li, X. Liang, Y. Wei, T. Xu, J. Feng, and S. Yan, "Perceptual generative adversarial networks for small object detection," in *CVPR*, 2017.
- [24] X. Wang, A. Shrivastava, and A. Gupta, "A-fast-rcnn: Hard positive generation via adversary for object detection," in *CVPR*, 2017.
- [25] A. Atapour-Abarghouei and T. P. Breckon, "Real-time monocular depth estimation using synthetic data with domain adaptation via image style transfer," in *CVPR*, 2018.
- [26] L. Tran, K. Sohn, X. Yu, X. Liu, and M. Chandraker, "Gotta adapt'em all: Joint pixel and feature-level domain adaptation for recognition in the wild," in *CVPR*, 2019.
- [27] B. Pan, Z. Cao, E. Adeli, and J. C. Niebles, "Adversarial cross-domain action recognition with co-attention," in *AAAI*, 2020.
- [28] X. Li, X. Yao, and Y. Fang, "Building-a-nets: Robust building extraction from high-resolution remote sensing images with adversarial networks," *IEEE Journal of Selected Topics in Applied Earth Observations and Remote Sensing*, vol. 11, no. 10, pp. 3680–3687, 2018.
- [29] B. Bischke, P. Helber, F. Koenig, D. Borth, and A. Dengel, "Overcoming missing and incomplete modalities with generative adversarial networks for building footprint segmentation," in *2018 International Conference on Content-Based Multimedia Indexing (CBMI)*. IEEE, 2018, pp. 1–6.
- [30] A. Abdollahi, B. Pradhan, S. Gite, and A. Alamri, "Building footprint extraction from high resolution aerial images using generative adversarial

network (gan) architecture,” *IEEE Access*, vol. 8, pp. 209 517–209 527, 2020.

- [31] X. Pan, F. Yang, L. Gao, Z. Chen, B. Zhang, H. Fan, and J. Ren, “Building extraction from high-resolution aerial imagery using a generative adversarial network with spatial and channel attention mechanisms,” *Remote Sensing*, vol. 11, no. 8, p. 917, 2019.
- [32] Y. Shi, Q. Li, and X. X. Zhu, “Building footprint generation using improved generative adversarial networks,” *IEEE Geoscience and Remote Sensing Letters*, vol. 16, no. 4, pp. 603–607, 2018.
- [33] H. A. Atabay, “Binary shape classification using convolutional neural networks,” *IIOAB J*, vol. 7, no. 5, pp. 332–336, 2016.
- [34] H. Ravishankar, R. Venkataramani, S. Thiruvankadam, P. Sudhakar, and V. Vaidya, “Learning and incorporating shape models for semantic segmentation,” in *International conference on medical image computing and computer-assisted intervention*. Springer, 2017, pp. 203–211.
- [35] T. Takikawa, D. Acuna, V. Jampani, and S. Fidler, “Gated-scnn: Gated shape cnns for semantic segmentation,” in *Proceedings of the IEEE/CVF International Conference on Computer Vision*, 2019, pp. 5229–5238.
- [36] W. Kuo, A. Angelova, J. Malik, and T.-Y. Lin, “Shapemask: Learning to segment novel objects by refining shape priors,” in *Proceedings of the IEEE/CVF International Conference on Computer Vision*, 2019, pp. 9207–9216.
- [37] H. Ding, X. Jiang, B. Shuai, A. Q. Liu, and G. Wang, “Semantic correlation promoted shape-variant context for segmentation,” in *Proceedings of the IEEE/CVF Conference on Computer Vision and Pattern Recognition*, 2019, pp. 8885–8894.
- [38] J. Liang, N. Homayounfar, W.-C. Ma, Y. Xiong, R. Hu, and R. Urtasun, “Polytransform: Deep polygon transformer for instance segmentation,” in *Proceedings of the IEEE/CVF Conference on Computer Vision and Pattern Recognition*, 2020, pp. 9131–9140.
- [39] L.-C. Chen, Y. Zhu, G. Papandreou, F. Schroff, and H. Adam, “Encoder-decoder with atrous separable convolution for semantic image segmentation,” in *ECCV*, 2018.
- [40] L. Ding, H. Tang, and L. Bruzzone, “Lanet: Local attention embedding to improve the semantic segmentation of remote sensing images,” *IEEE Transactions on Geoscience and Remote Sensing*, 2020.
- [41] K. He, X. Zhang, S. Ren, and J. Sun, “Deep residual learning for image recognition,” in *CVPR*, 2016.
- [42] P. Liu, X. Liu, M. Liu, Q. Shi, J. Yang, X. Xu, and Y. Zhang, “Building footprint extraction from high-resolution images via spatial residual inception convolutional neural network,” *Remote Sensing*, vol. 11, no. 7, p. 830, 2019.
- [43] L. Ding and L. Bruzzone, “Diresnet: Direction-aware residual network for road extraction in vhr remote sensing images,” *IEEE Transactions on Geoscience and Remote Sensing*, 2020.
- [44] L. Ding, J. Zhang, and L. Bruzzone, “Semantic segmentation of large-size vhr remote sensing images using a two-stage multiscale training architecture,” *IEEE Transactions on Geoscience and Remote Sensing*, 2020.
- [45] X. Zhu, H. Hu, S. Lin, and J. Dai, “Deformable convnets v2: More deformable, better results,” in *Proceedings of the IEEE/CVF Conference on Computer Vision and Pattern Recognition*, 2019, pp. 9308–9316.
- [46] S. Ye, R. G. Pontius Jr, and R. Rakshit, “A review of accuracy assessment for object-based image analysis: From per-pixel to per-polygon approaches,” *ISPRS Journal of Photogrammetry and Remote Sensing*, vol. 141, pp. 137–147, 2018.
- [47] I. Lizarazo, “Accuracy assessment of object-based image classification: another step,” *International Journal of Remote Sensing*, vol. 35, no. 16, pp. 6135–6156, 2014.
- [48] E. Maggiori, Y. Tarabalka, G. Charpiat, and P. Alliez, “Can semantic labeling methods generalize to any city? the inria aerial image labeling benchmark,” in *2017 IEEE International Geoscience and Remote Sensing Symposium (IGARSS)*. IEEE, 2017, pp. 3226–3229.
- [49] V. Mnih, “Machine learning for aerial image labeling,” Ph.D. dissertation, University of Toronto, 2013.
- [50] C. Persello and L. Bruzzone, “A novel protocol for accuracy assessment in classification of very high resolution images,” *IEEE Transactions on Geoscience and Remote Sensing*, vol. 48, no. 3, pp. 1232–1244, 2010.
- [51] R. C. Gonzalez and R. E. Woods, “Digital image processing. upper saddle river,” *J. Prentice Hall*, 2002.



**Lei Ding** received the B.S. degree in Measurement and Control Engineering in 2013 and the M.S. degree in Photogrammetry and Remote Sensing in 2016, both from University of Information Engineering, Zhengzhou, China. He is currently pursuing the Ph.D. degree at RSLab in the Department of Information Engineering and Computer Science, University of Trento, Italy. His research interests are related to remote sensing image processing, and machine learning.



**Hao Tang** is a Ph.D. candidate in the Department of Information Engineering and Computer Science at the University of Trento. He received the Master degree in computer application technology in 2016 at the School of Electronics and Computer Engineering, Peking University. He was a visiting scholar in the Department of Engineering Science at the University of Oxford, from 2019 to 2020. His research interests are deep learning, machine learning, and their applications to computer vision.



**Yahui Liu** is a Ph.D. student in the Department of Information Engineering and Computer Science at the University of Trento, Italy. Before that, he received his B.S. degree and M.S. degree from Wuhan University, China, in 2015 and 2018, respectively. His major research interests are machine learning and computer vision, including unsupervised learning and image domain translation.



**Lorenzo Bruzzone** (S'95-M'98-SM'03-F'10) received the Laurea (M.S.) degree in electronic engineering (*summa cum laude*) and the Ph.D. degree in telecommunications from the University of Genoa, Italy, in 1993 and 1998, respectively.

He is currently a Full Professor of telecommunications at the University of Trento, Italy, where he teaches remote sensing, radar, and digital communications. Dr. Bruzzone is the founder and the director of the Remote Sensing Laboratory in the Department of Information Engineering and Computer Science,

University of Trento. His current research interests are in the areas of remote sensing, radar and SAR, signal processing, machine learning and pattern recognition. He promotes and supervises research on these topics within the frameworks of many national and international projects. He is the Principal Investigator of many research projects. Among the others, he is the Principal Investigator of the *Radar for icy Moon exploration* (RIME) instrument in the framework of the *Jupiter ICy moons Explorer* (JUICE) mission of the European Space Agency. He is the author (or coauthor) of 215 scientific publications in referred international journals (154 in IEEE journals), more than 290 papers in conference proceedings, and 21 book chapters. He is editor/co-editor of 18 books/conference proceedings and 1 scientific book. He was invited as keynote speaker in more than 30 international conferences and workshops. Since 2009 he is a member of the Administrative Committee of the IEEE Geoscience and Remote Sensing Society (GRSS).

Dr. Bruzzone was a Guest Co-Editor of many Special Issues of international journals. He is the co-founder of the IEEE International Workshop on the Analysis of Multi-Temporal Remote-Sensing Images (MultiTemp) series and is currently a member of the Permanent Steering Committee of this series of workshops. Since 2003 he has been the Chair of the SPIE Conference on Image and Signal Processing for Remote Sensing. He has been the founder of the IEEE Geoscience and Remote Sensing Magazine for which he has been Editor-in-Chief between 2013-2017. Currently he is an Associate Editor for the IEEE Transactions on Geoscience and Remote Sensing. He has been Distinguished Speaker of the IEEE Geoscience and Remote Sensing Society between 2012-2016. His papers are highly cited, as proven from the total number of citations (more than 27000) and the value of the h-index (78) (source: Google Scholar).